12

Excitation of discrete states in (e, e')

Consider the simplest case of excitation of a discrete state of the target in inclusive electron scattering (e, e'). The kinematics are illustrated in Fig. 12.1. If $M_T^\star$ is the final target mass, then

$$\begin{aligned} p' &= p - q \\ -M_T^{\star 2} &= -M_T^2 - 2p \cdot q + q^2 \\ 2p \cdot q &= M_T^{\star 2} - M_T^2 + q^2 \\ &= 2M_T(\varepsilon_1 - \varepsilon_2) \end{aligned} \tag{12.1}$$

The last relation evaluates $p \cdot q = -M_T q_0$ in the laboratory frame. One observes that here only q^2 is an independent variable.

The integral over the energy-conserving delta function appearing in the response tensor can be performed according to

$$\begin{aligned} \int d\varepsilon_2 \delta(E' - M_T + q_0) &= \int d\varepsilon_2 \delta(W_f - W_i) \\ &= \int dW_f \, \delta(W_f - W_i) \left(\frac{\partial \varepsilon_2}{\partial W_f} \right) \\ &= \left(\frac{\partial \varepsilon_2}{\partial W_f} \right) \qquad ; W_i = M_T + \varepsilon_1 \end{aligned} \tag{12.2}$$

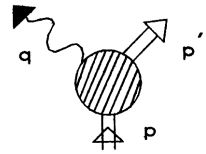

Fig. 12.1. Kinematics in inclusive electron scattering.

https://doi.org/10.1017/9781009290616.015 Published online by Cambridge University Press

This jacobian is evaluated as follows

$$\begin{aligned} W_f &= (\mathbf{p}'^2 + M_T^{\star 2})^{1/2} + \varepsilon_2 \\ &= [(\mathbf{k}_1 - \mathbf{k}_2)^2 + M_T^{\star 2}]^{1/2} + \varepsilon_2 \\ &= [\varepsilon_1^2 + \varepsilon_2^2 - 2\varepsilon_1\varepsilon_2 \cos\theta + M_T^{\star 2}]^{1/2} + \varepsilon_2 \\ \frac{\partial W_f}{\partial \varepsilon_2} &= \frac{\varepsilon_2 - \varepsilon_1 \cos\theta}{E'} + 1 \\ &= \frac{\varepsilon_2 + E' - \varepsilon_1 \cos\theta}{E'} = \frac{M_T + \varepsilon_1 - \varepsilon_1 \cos\theta}{E'} \\ &= \frac{M_T}{E'}\left[1 + \frac{2\varepsilon_1 \sin^2(\theta/2)}{M_T}\right] \end{aligned} \tag{12.3}$$

Energy conservation has been used. The inverse of this relation gives the required result

$$\begin{aligned} \frac{\partial \varepsilon_2}{\partial W_f} &= \frac{E'}{M_T} r \\ r^{-1} &\equiv \left[1 + \frac{2\varepsilon_1 \sin^2(\theta/2)}{M_T}\right] \end{aligned} \tag{12.4}$$

Take out the following Lorentz invariant factors from the coefficients in the response tensor

$$W_i(q^2, q\cdot p) \equiv w_i(q^2)\frac{M_T^2}{E'}\delta(p_0 - p_0' - q_0) \qquad ; i = 1, 2 \tag{12.5}$$

Then, from the above,

$$\int \frac{d\varepsilon_2}{M_T} W_i(q^2, q\cdot p) = w_i(q^2)\, r \tag{12.6}$$

The remaining response tensor, which will be denoted by $w_{\mu\nu}$, is given by

$$w_{\mu\nu}(q^2) = \overline{\sum}_i \sum_f \frac{E E' \Omega}{M_T^2}(2\pi)^3 \delta^{(3)}(\mathbf{p} - \mathbf{p}' - \mathbf{q}) \langle i|J_\nu(0)|f\rangle\langle f|J_\mu(0)|i\rangle \tag{12.7}$$

The sum over final states in the continuum limit takes the form

$$\sum_f \to \sum_f{}' \frac{\Omega\, d^3p'}{(2\pi)^3} \tag{12.8}$$

Here $\sum_f{}'$ now goes over all other quantum numbers. The final result for the Lorentz invariant response tensor in this discrete case can then be

https://doi.org/10.1017/9781009290616.015 Published online by Cambridge University Press

written

$$w_{\mu\nu}(q^2) = \overline{\sum_i} \sum_f{}' \frac{EE'\Omega^2}{M_T^2} \langle i|J_\nu(0)|f\rangle\langle f|J_\mu(0)|i\rangle \tag{12.9}$$
$$= w_1(q^2)\left(\delta_{\mu\nu} - \frac{q_\mu q_\nu}{q^2}\right) + w_2(q^2)\frac{1}{M_T^2}\left(p_\mu - \frac{p\cdot q}{q^2}q_\mu\right)\left(p_\nu - \frac{p\cdot q}{q^2}q_\nu\right)$$

This relation allows an identification of the transition form factors $w_{1,2}(q^2)$. The variables q^2 and $q\cdot p$ are here related through Eq. (12.1). Furthermore, a combination of Eqs. (11.38, 12.6) yields the cross section

$$\frac{d\sigma}{d\Omega} = \sigma_M \left[w_2(q^2) + 2w_1(q^2)\tan^2\frac{\theta}{2}\right] r \tag{12.10}$$

This is an exact result, to order α^2, for the scattering of a relativistic electron with corresponding excitation of a discrete state in any quantum mechanical target.

As a simple example, consider elastic scattering from a $J^\pi = 0^+$ target. The kinematics in Eq. (12.1) yields for elastic scattering

$$\begin{aligned} M_T^\star &= M_T \equiv m \\ 2p\cdot q &= q^2 \end{aligned} \tag{12.11}$$

From Lorentz covariance and current conservation, one can write the general form of the matrix element of the current in this case as

$$\langle p'\,;0^+|J_\mu(0)|p\,;0^+\rangle = \left(\frac{m^2}{EE'\Omega^2}\right)^{1/2} F_0(q^2)\frac{1}{m}\left(p_\mu - \frac{p\cdot q}{q^2}q_\mu\right) \tag{12.12}$$

Hence one can simply read off from Eqs. (12.9)

$$\begin{aligned} w_1 &= 0 \\ w_2 &= |F_0(q^2)|^2 \end{aligned} \tag{12.13}$$

As a second example, consider elastic scattering from a $J^\pi = 1/2^+$ target. It follows from Lorentz covariance and current conservation that the most general form of the matrix element of the current in this case is given by [Bj65]

$$\langle\, p'\,;1/2^+|J_\mu(0)|\,p\,;1/2^+\rangle = \frac{i}{\Omega}\bar{u}(p')\left[F_1(q^2)\gamma_\mu + F_2(q^2)\sigma_{\mu\nu}q_\nu\right]u(p)$$
$$\sigma_{\mu\nu} \equiv \frac{1}{2i}[\gamma_\mu, \gamma_\nu] \tag{12.14}$$

https://doi.org/10.1017/9781009290616.015 Published online by Cambridge University Press

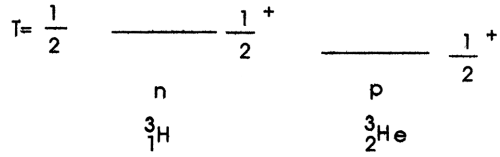

Fig. 12.2. Elastic scattering from isodoublets.

This time one has to do a little work, but with the aid of the positive energy projection operator, and by taking the resulting traces, one identifies

$$\begin{aligned} w_1(q^2) &= \frac{q^2}{4m^2}|F_1 + 2mF_2|^2 \\ w_2(q^2) &= |F_1|^2 + \frac{q^2}{4m^2}|2mF_2|^2 \end{aligned} \tag{12.15}$$

Substitution in Eq. (12.10) then yields the celebrated *Rosenbluth cross section*. Although very instructive, we leave the derivation of Eqs. (12.14, 12.15) to the dedicated reader.[1]

The Rosenbluth cross section is quite general. It of course applies to the nucleon, the isodoublet (p, n). It also applies to the nuclear isodoublet $({}^3_2\mathrm{He}, {}^3_1\mathrm{H})$ as illustrated in Fig. 12.2. In both cases, one can actually do elastic scattering experiments on the higher energy state. In the case of the neutron, one uses a deuteron ${}^2_1\mathrm{H}$ in which the neutron is bound to a proton. In the case of tritium ${}^3_1\mathrm{H}$, this nucleus lives long enough that one can make targets of it for external beam experiments.

It is useful to make the isospin dependence of the form factor manifest in the case of scattering from an isodoublet target. The general isospin structure of the electromagnetic current operator in any description of nuclei and nucleons (mesons and baryons, quarks and gluons, etc.) is

$$J^\gamma_\mu = J^S_\mu + J^{V_3}_\mu \tag{12.16}$$

Here the superscript describes the behavior under isospin transformations, either scalar or third component of an isovector. It follows from the Wigner–Eckart theorem that the matrix elements of the current must reflect that behavior. Thus the form factors must have the structure

$$F_i = \frac{1}{2}(F^S_i + F^V_i \tau_3) \qquad ; i = 1, 2 \tag{12.17}$$

Here $\boldsymbol{\tau}$ are the Pauli matrices, and the target isospinors are suppressed in

[1] Hermiticity of the current implies that the form factors in these examples are real.

https://doi.org/10.1017/9781009290616.015 Published online by Cambridge University Press

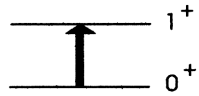

Fig. 12.3. Inelastic transition $0^+ \to 1^+$.

Eq. (12.14). For the nucleon, it follows that

$$\begin{aligned} F_i^p &= \frac{1}{2}(F_i^S + F_i^V) & F_i^S &= F_i^p + F_i^n \\ F_i^n &= \frac{1}{2}(F_i^S - F_i^V) & F_i^V &= F_i^p - F_i^n \end{aligned} \tag{12.18}$$

It is useful to summarize the following numerical values for the nucleon ($m \equiv m_p$)

$$\begin{aligned} F_1^p(0) &= 1 & F_1^S(0) &= 1 \\ F_1^n(0) &= 0 & F_1^V(0) &= 1 \\ 2mF_2^p(0) &= +1.793 & 2mF_2^S(0) &= -.120 \\ 2mF_2^n(0) &= -1.913 & 2mF_2^V(0) &= +3.706 \end{aligned} \tag{12.19}$$

Consider next an inelastic transition $0^+ \to 1^+$ as illustrated in Fig. 12.3. From Lorentz covariance, the general form of the transition matrix element of the current can be written as

$$\langle p'; 1^+\lambda | J_\mu(0) | p; 0^+ \rangle = \left(\frac{mm^\star}{EE'\Omega^2} \right)^{1/2} \frac{f(q^2)}{\sqrt{2}\, mm^\star} \varepsilon_{\mu\nu\rho\sigma}\, \varepsilon_\nu^{(\lambda)\star} p_\rho q_\sigma \tag{12.20}$$

Here λ is the helicity of the final 1^+ particle, and its polarization four-vector is given by

$$\varepsilon_\nu^{(\lambda)\star} \equiv (\boldsymbol{\varepsilon}^{(\lambda)\dagger},\ i\varepsilon_0^{(\lambda)\dagger}) \tag{12.21}$$

Because of the intrinsic parity of the 1^+ particle, this matrix element must transform as an axial vector. Note that current conservation is automatically maintained since $q_\mu \varepsilon_{\mu\nu\rho\sigma} q_\sigma = 0$.

To calculate the cross section one needs the sum over polarization vectors, which for a spin one particle is given by[2]

$$\sum\nolimits_\lambda \varepsilon_\mu^{(\lambda)\star} \varepsilon_\nu^{(\lambda)} = \delta_{\mu\nu} + \frac{p'_\mu p'_\nu}{m^{\star 2}} \tag{12.22}$$

[2] This must be a second rank tensor, and the polarization vectors satisfy $p' \cdot \varepsilon^{(\lambda)} = 0$.

https://doi.org/10.1017/9781009290616.015 Published online by Cambridge University Press

After some algebra, one then obtains

$$\begin{aligned} w_1 &= \frac{\mathbf{q}^2}{2mm^\star}|f(q^2)|^2 \\ w_2 &= \frac{q^2}{2mm^\star}|f(q^2)|^2 \end{aligned} \tag{12.23}$$

The cross section then follows from Eq. (12.10). We shall see from the subsequent multipole analysis that this represents a "pure M1 cross section."

The reader can now write his or her own "elementary cross section." Just pick a transition and use Lorentz covariance and current conservation to write the general form of the matrix element of the current. The response functions $w_{1,2}(q^2)$ are then identified from Eqs. (12.9) and the cross section from Eq. (12.10).

Let us now make a connection to the analysis of real photon transitions in chapter 9 and make a *multipole analysis* of the electron scattering cross section. We start by going back a step and restoring the spatial dependence to the matrix elements in Eq. (11.20) through the use of the Heisenberg equations of motion

$$\begin{aligned} W_{\mu\nu} &= \overline{\sum_i}\sum_f \delta(p_0 - p_0' - q_0)\langle i|\int e^{i\mathbf{q}\cdot\mathbf{x}}J_\nu(\mathbf{x})\,d^3x|f\rangle \\ &\quad \times\langle f|\int e^{-i\mathbf{q}\cdot\mathbf{x}}J_\mu(\mathbf{x})\,d^3x|i\rangle(E) \end{aligned} \tag{12.24}$$

This relation is still exact since if the initial and final states are eigenstates of momentum, one has

$$\begin{aligned} \langle f|\int e^{-i\mathbf{q}\cdot\mathbf{x}}J_\mu(\mathbf{x})\,d^3x|i\rangle &= \Omega\delta_{\mathbf{p},\mathbf{p}'+\mathbf{q}}\langle f|J_\mu(0)|i\rangle \\ \text{and then;}\quad \langle i|\int e^{i\mathbf{q}\cdot\mathbf{x}}J_\nu(\mathbf{x})\,d^3x|f\rangle &= \Omega\langle i|J_\nu(0)|f\rangle \end{aligned} \tag{12.25}$$

Thus in the limit $\Omega \to \infty$

$$W_{\mu\nu} = (2\pi)^3\overline{\sum_i}\sum_f \delta^{(4)}(p - p' - q)\langle i|J_\nu(0)|f\rangle\langle f|J_\mu(0)|i\rangle(E\,\Omega) \tag{12.26}$$

This is our previous result.

Assume one goes to a discrete state with mass $M_T^\star$, then just as before

$$W_{\mu\nu} \equiv \frac{M_T^2}{E'}\delta(p_0 - p_0' - q_0)w_{\mu\nu} \tag{12.27}$$

$$\begin{aligned} w_{\mu\nu} &= \overline{\sum_i}\sum_f\left(\frac{EE'}{M_T^2}\right)\langle i|\int e^{i\mathbf{q}\cdot\mathbf{x}}J_\nu(\mathbf{x})\,d^3x|f\rangle\langle f|\int e^{-i\mathbf{q}\cdot\mathbf{x}}J_\mu(\mathbf{x})\,d^3x|i\rangle \\ &= w_1(q^2)\left(\delta_{\mu\nu} - \frac{q_\mu q_\nu}{q^2}\right) + w_2(q^2)\frac{1}{M_T^2}\left(p_\mu - \frac{p\cdot q}{q^2}q_\mu\right)\left(p_\nu - \frac{p\cdot q}{q^2}q_\nu\right) \end{aligned}$$

The cross section is again given by Eq. (12.10).

https://doi.org/10.1017/9781009290616.015 Published online by Cambridge University Press

Let us now solve Eqs. (12.27) for the functions $w_{1,2}(q^2)$. First take $\mu = \nu = 4$ and make use of the fact that in the laboratory frame $p = (\mathbf{0}, iM_T)$. This yields

$$w_1\left(1+\frac{q_0^2}{q^2}\right) - w_2\left(1+\frac{q_0^2}{q^2}\right)^2 = w_1\frac{\mathbf{q}^2}{q^2} - w_2\frac{\mathbf{q}^4}{q^4}$$
$$= -\overline{\sum_i}\sum_f \left(\frac{EE'}{M_T^2}\right)|\langle f|\int e^{-i\mathbf{q}\cdot\mathbf{x}}\hat{\rho}(\mathbf{x})\,d^3x|i\rangle|^2 \tag{12.28}$$

Next dot the spatial part of the tensor $W_{\mu\nu}$ into the spherical unit vectors $\mathbf{e}_{\mathbf{q}\lambda}$ from the left and $\mathbf{e}^\dagger_{\mathbf{q}\lambda}$ from the right. Here these spherical unit vectors are defined with respect to the direction of the momentum transfer $\mathbf{q}$ [see Fig. 8.1 and Eqs. (8.4)]. For $\lambda = \pm 1$ they satisfy

$$\begin{aligned} \mathbf{e}_{\mathbf{q}\lambda}\cdot\mathbf{e}^\dagger_{\mathbf{q}\lambda} &= 1 \\ \mathbf{e}_{\mathbf{q}\lambda}\cdot\mathbf{q} &= 0 \qquad ;\lambda = \pm 1 \end{aligned} \tag{12.29}$$

As a result of these observations, the term in w_2 no longer contributes. Finally, take $\sum_{\lambda=\pm1}$ to simplify things. The result of these operations is

$$2w_1 = \sum_{\lambda=\pm1}\overline{\sum_i}\sum_f \left(\frac{EE'}{M_T^2}\right)|\langle f|\int e^{-i\mathbf{q}\cdot\mathbf{x}}\,\mathbf{e}^\dagger_{\mathbf{q}\lambda}\cdot\hat{\mathbf{J}}(\mathbf{x})\,d^3x|i\rangle|^2 \tag{12.30}$$

These equations can now be solved for $w_{1,2}(q^2)$ with the result

$$2w_1(q^2) = \sum_{\lambda=\pm1}\overline{\sum_i}\sum_f \left(\frac{EE'}{M_T^2}\right)|\langle f|\int e^{-i\mathbf{q}\cdot\mathbf{x}}\,\mathbf{e}^\dagger_{\mathbf{q}\lambda}\cdot\hat{\mathbf{J}}(\mathbf{x})\,d^3x|i\rangle|^2 \tag{12.31}$$
$$w_2(q^2) = \frac{q^2}{\mathbf{q}^2}w_1(q^2) + \frac{q^4}{\mathbf{q}^4}\overline{\sum_i}\sum_f \left(\frac{EE'}{M_T^2}\right)|\langle f|\int e^{-i\mathbf{q}\cdot\mathbf{x}}\,\hat{\rho}(\mathbf{x})\,d^3x|i\rangle|^2$$

These equations are still exact.

Now assume, just as in the analysis of real photon transitions in chapters 8 and 9, that

- The target is heavy and the transition densities are well localized in space
- The initial and final states are eigenstates of angular momentum

Thus one imagines that the target is heavy and "nailed down" (at the origin, say). It makes a transition, and the localized transition density scatters the electron. Here target recoil (i.e. the C-M motion of the target)

https://doi.org/10.1017/9781009290616.015 Published online by Cambridge University Press

is neglected in the transition matrix elements;[3] it is included correctly where it is most important through the recoil phase space factor r.

The multipole analysis now proceeds exactly as in chapter 9. The essential difference is that the argument of the spherical Bessel functions in the multipoles, instead of being given by $|\mathbf{k}|$ the momentum of the photon (with $|\mathbf{k}| = \omega$), is now given by $\kappa = |\mathbf{q}|$ the momentum transfer in the electron scattering process.

$$\kappa \equiv |\mathbf{q}| \tag{12.32}$$

In addition to the transverse electric and magnetic multipoles of Eq. (9.11)

$$\begin{aligned} \hat{T}^{\rm el}_{JM}(\kappa) &\equiv \frac{1}{\kappa}\int d^3x \left[\nabla \times j_J(\kappa x)\mathscr{Y}^M_{JJ1}(\Omega_x)\right]\cdot\hat{\mathbf{J}}(\mathbf{x}) \\ \hat{T}^{\rm mag}_{JM}(\kappa) &\equiv \int d^3x \left[j_J(\kappa x)\mathscr{Y}^M_{JJ1}(\Omega_x)\right]\cdot\hat{\mathbf{J}}(\mathbf{x}) \end{aligned} \tag{12.33}$$

there is now a Coulomb multipole of the charge density defined by

$$\hat{M}_{JM}(\kappa) \equiv \int d^3x\, j_J(\kappa x) Y_{JM}(\Omega_x)\,\hat{\rho}(\mathbf{x}) \tag{12.34}$$

This is the same multipole that appears at long wavelength in the expansion of $\hat{T}^{\rm el}_{JM}(k)$ in Eq. (A.13).

The use of the Wigner–Eckart theorem allows one to do the sum and average over nuclear states, and exactly as in chapter 9 one arrives at the relations

$$\begin{aligned} 2w_1(q^2) &= \frac{E'}{M_T}\frac{4\pi}{2J_i+1}\sum_{J\geq 1}\left\{|\langle J_f||\hat{T}^{\rm mag}_J(\kappa)||J_i\rangle|^2 + |\langle J_f||\hat{T}^{\rm el}_J(\kappa)||J_i\rangle|^2\right\} \\ w_2(q^2) &= \frac{q^2}{\mathbf{q}^2}w_1(q^2) + \frac{q^4}{\mathbf{q}^4}\frac{E'}{M_T}\frac{4\pi}{2J_i+1}\sum_{J\geq 0}|\langle J_f||\hat{M}_J(\kappa)||J_i\rangle|^2 \end{aligned} \tag{12.35}$$

The Wigner–Eckart theorem limits the sums on multipoles appearing in these expressions to values satisfying the triangle inequality $|J_f - J_i| \leq J \leq J_f + J_i$.

The cross section follows from Eq. (12.10) as

$$\begin{aligned} \frac{d\sigma}{d\Omega} &= \sigma_M \frac{4\pi}{2J_i+1}\left\{\frac{q^4}{\mathbf{q}^4}\sum_{J\geq 0}|\langle J_f||\hat{M}_J(\kappa)||J_i\rangle|^2\right. \\ &\left. + \left(\frac{q^2}{2\mathbf{q}^2} + \tan^2\frac{\theta}{2}\right)\sum_{J\geq 1}\left(|\langle J_f||\hat{T}^{\rm mag}_J(\kappa)||J_i\rangle|^2 + |\langle J_f||\hat{T}^{\rm el}_J(\kappa)||J_i\rangle|^2\right)\right\}\bar{r} \end{aligned} \tag{12.36}$$

[3] The C-M motion can, in fact, be handled correctly in the usual non-relativistic nuclear physics problem using, for example, the approach in appendix A of [Fo69]. We reproduce that analysis here in appendix B.

https://doi.org/10.1017/9781009290616.015 Published online by Cambridge University Press

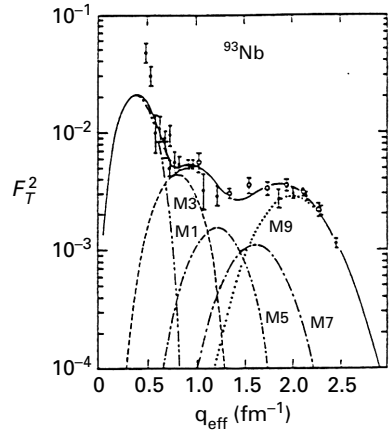

Fig. 12.4. Elastic magnetic scattering response F_T^2 for $^{93}_{41}$Nb(e, e). Here $q_{\text{eff}} \equiv \kappa$. The single-particle shell model configuration assignment is $(1g_{9/2})_\pi$. The work is from Bates [Yo79].

Here the recoil factor $\bar{r}$ is given by

$$\begin{aligned}(\bar{r})^{-1} &\equiv \frac{M_T}{E'} r^{-1} \\ &= \frac{1}{E'}(M_T + \varepsilon_1 - \varepsilon_1 \cos\theta) \\ &= 1 + \frac{(\varepsilon_2 - \varepsilon_1 \cos\theta)}{E'} \end{aligned} \tag{12.37}$$

Energy conservation has been used in obtaining this result (note that for most nuclear applications $M_T/E' \approx 1$).

Equation (12.36) is the general electron scattering cross section, to order α^2, from an arbitrary, localized quantum mechanical target. It forms the basis for much of our future discussion. To give the reader some feel for these results, we briefly present a few selected applications.

For real photon transitions, it is the *lowest* allowed multipole that dominates the transition (appendix A). One of the most intriguing features of electron scattering (e, e′) is that by increasing the momentum transfer κ, one can in essence dial the contributing multipolarity, even to the extent that it is the *highest* allowed multipole that dominates. We give three examples.

Figure 12.4 shows elastic magnetic scattering from $^{93}_{41}$Nb(e, e). This represents the contribution to the cross section from the transverse multipoles in the second line of Eq. (12.36). This contribution can be separated experimentally by making a straight-line *Rosenbluth plot* against $\tan^2(\theta/2)$ at fixed q^2, or by working at $\theta = 180^\circ$ where only the transverse term

https://doi.org/10.1017/9781009290616.015 Published online by Cambridge University Press

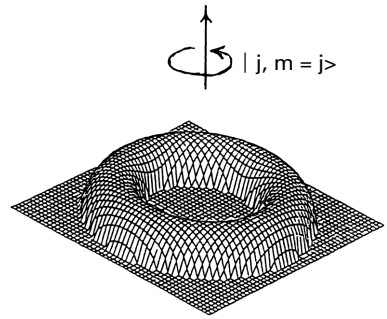

Fig. 12.5. Surface of $\mu(x)_{\max}/2$ for $^{51}_{23}$V with configuration assignment $(1f_{7/2})_\pi$ plotted on a 10 fm square. Here the angular momentum is aligned along the z-axis with $m_j = j$ [Do73].

contributes.[4] Parity and time-reversal invariance of the strong interactions limit one to the odd transverse magnetic multipoles in elastic scattering.[5] The work shown is from Bates [Yo79]. The single-particle shell model configuration assignment for $^{93}_{41}$Nb is $(1g_{9/2})_\pi$; recall it is predominantly the valence nucleon that gives rise to the magnetic properties of nuclei. Note how at long wavelength (low κ) the transition is all M1, while each higher multipole dominates in turn as κ is increased, until at high κ it is all M9.

What does one learn from this? Figure 12.5 shows the surface of half-maximum intrinsic magnetization density $\mu(x)_{\max}/2$ for $^{51}_{23}$V (chosen so that it would fit on a 10 fm square). Here the configuration assignment is $(1f_{7/2})_\pi$, and the nucleus is aligned so that its angular momentum points along the z-axis with $m_j = j$. The intrinsic magnetization tracks the location of the valence nucleon. The nucleus is a small magnet with a current loop provided by the motion of the orbiting proton. Elastic magnetic electron scattering at all κ provides a microscope to actually see the spatial structure of this small current loop [Do73].

We next recall that one of the distinguishing features of the shell model, for whose discovery Mayer and Jensen won the Nobel prize, is that levels with the highest angular momentum and opposite parity from one major shell are pushed down close to the levels of the next lower major shell. If that lower shell is filled (or partially filled), one can have low-lying, high-spin, magnetic, particle–hole transitions of the nucleus. Figure 12.6 shows

[4] The notation used here is $d\sigma/d\Omega \equiv \sigma_M[(q^4/\mathbf{q}^4)F_L^2 + (q^2/2\mathbf{q}^2 + \tan^2\theta/2)F_T^2]r$.

[5] An analysis similar to that for parity in chapter 9 shows that the time-reversal behavior (which includes complex conjugation) of both of the transverse multipoles is $\hat{\mathscr{T}}\hat{T}_{JM}\hat{\mathscr{T}}^{-1} = (-1)^{J+1}\hat{T}_{J-M}$. This, combined with the hermiticity of the current, leads to the quoted selection rule in the elastic case [Pr65, Do73] — see appendix E.

https://doi.org/10.1017/9781009290616.015 Published online by Cambridge University Press

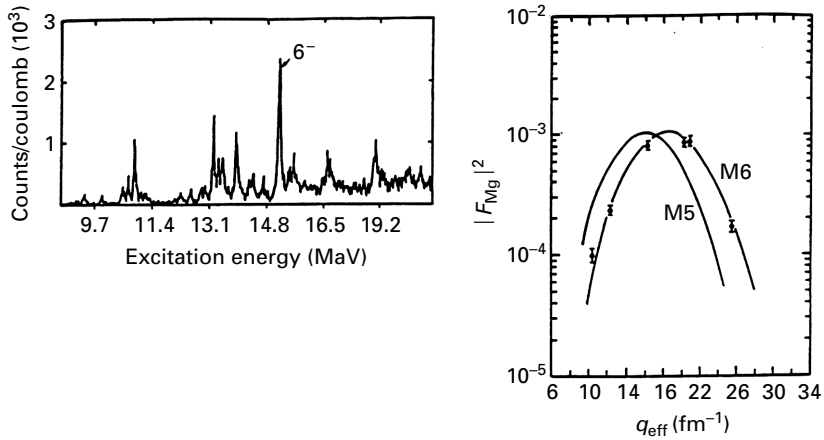

Fig. 12.6. Transverse response for $^{24}_{12}\mathrm{Mg}(\mathrm{e},\mathrm{e}')$ at $\theta = 160^{\circ}$ and $\kappa = 2.13\,\mathrm{fm}^{-1}$ with the 6^- indicated. Also shown is the inelastic form factor F_T^2 for the 6^-, defined to be the area under the inelastic peak, vs. $\kappa \equiv q_{\mathrm{eff}}$. This quantity is compared with the theoretical result (open-shell RPA) for a transition to the $[1f_{7/2}(1d_{5/2})^{-1}]_{6^-}$ state. The work is from Bates [Za77].

the large-angle, large κ response for electron excitation of $^{24}_{12}\mathrm{Mg}(\mathrm{e},\mathrm{e}')$. Also shown is the inelastic form factor, the area under the peak, as a function of κ for the dominant transition. This inelastic form factor manifests a characteristic M6 dependence, identifying the excited state as 6^-. The configuration assignment here is $1f_{7/2}(1d_{5/2})^{-1}$ and the 6^- is the *highest* J^π which can be formed from this configuration.[6] The work was done at Bates [Za77]. Excitations up to 14^- in $^{208}_{82}\mathrm{Pb}$ have been similarly studied [Li79].

As a third application, there are regions of the periodic table where nuclei are deformed. Bohr, Mottelson, and Rainwater won the Nobel prize for their analysis of these systems. Suppose one measures elastic scattering, and inelastic electron scattering, to all members of the ground-state rotational band, at all κ. This requires very good energy resolution, since the ground-state band for heavy nuclei is closely spaced, and involves bringing out all the transitions of increasing multipolarity in the rotational spectrum. It is then possible to actually *see the deformed charge distribution.* This is illustrated in Fig. 12.7. The work was done at Bates [He86]. The study of the intrinsic structure of deformed nuclei is one of the most important contributions of the Bates Laboratory.

[6] Note that the large J^π produces a very narrow state (this state lies above particle emission threshold). Furthermore, the large isovector magnetic moment of the nucleon in Eq. (12.19), through which the state is predominantly excited from the $T = 0$ ground state, implies this excited state has isospin $T = 1$.

https://doi.org/10.1017/9781009290616.015 Published online by Cambridge University Press

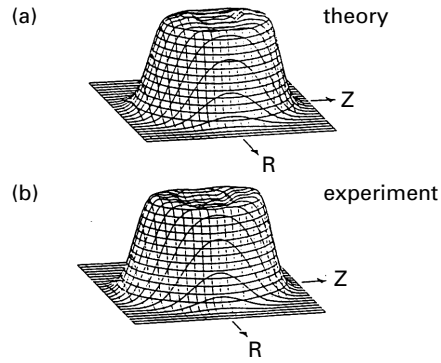

Fig. 12.7. Shape of charge distribution in the deformed nucleus $^{154}_{64}$Gd(e, e′) (b) from work at Bates; (a) deformed Hartree–Fock calculation of the same [He86].

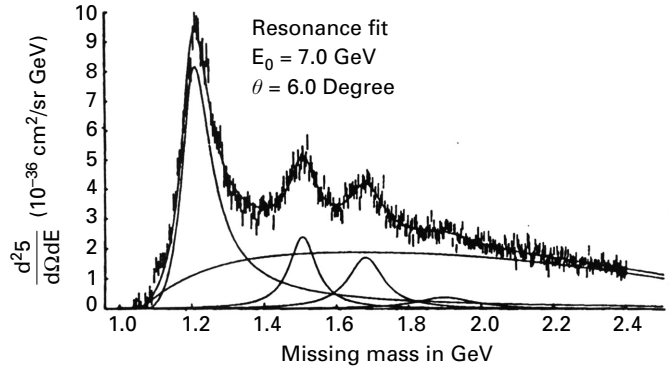

Fig. 12.8. Inelastic cross section for ^{1}H(e, e′) in the resonance region measured at SLAC with $\varepsilon_1 = 7.0\,\text{GeV}$ and $\theta = 6.0^\text{o}$. The elastic peak has been suppressed. Also shown are resonance and smooth background fits [Bl68].

As a fourth brief application, consider electron excitation of the nucleon itself. A general discussion of the process $(1/2^+, 1/2) \rightarrow (J^\pi, T)$ can be found in [Bj66].

Figure 12.8 shows the inelastic cross section for ^{1}H(e, e′) in the resonance region measured at SLAC [Bl68]. These results are even more impressive when one realizes that the elastic peak has been suppressed. Also shown in this figure is a Breit–Wigner resonance fit, together with a smooth, polynomial background [Bl68, Br71]. The first resonance, the $\Delta(1232)$ with $(J^\pi, T) = (3/2^+, 3/2)$, clearly stands out. The second peak consists of at least two levels. The third has several levels, and with a good stretch of the imagination, one can even discern a fourth peak.

Figure 12.9 shows the ratio $(d\sigma_\text{in}/d\sigma_\text{el})_{6^\text{o}}$ for ^{1}H(e, e′)$\Delta(1232)$ as measured by the SLAC–M.I.T. collaboration [Bl68, Br71]. The inelastic cross

https://doi.org/10.1017/9781009290616.015 Published online by Cambridge University Press

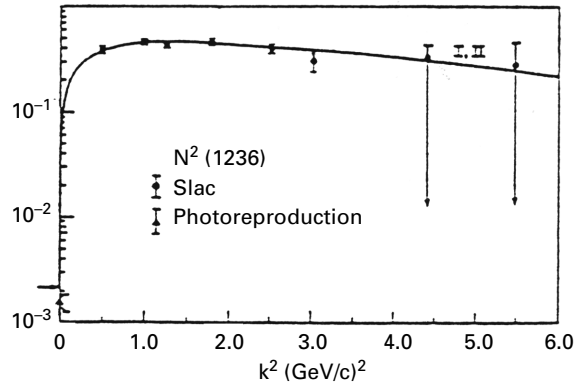

Fig. 12.9. Ratio $(d\sigma_{\text{in}}/d\sigma_{\text{el}})_{6^\circ}$ for ^{1}H(e, e′)Δ(1232) (see text) [Wa72]. Here $k^2 \equiv q^2$.

section for excitation of the resonance is obtained from the area under the resonance peak. The ratio to the elastic cross section is then plotted as a function of the four-momentum transfer q^2. Note that there is one point on this plot at $q^2 = 0$ obtained from photoabsorption.[7] The solid curve is a covariant, gauge-invariant calculation formulated in terms of hadronic degrees of freedom [Pr69, Wa72]. The calculation uses the multipole projections of the hadronic pole terms from (π, ω, N) exchange, with a resonant final-state enhancement factor determined from the π-N phase shift; it is discussed in some detail in chapter 28. This calculation can be viewed as a synthesis of a great deal of work on this process by Fubini Nambu and Wataghin [Fu58], Dennery [De61], Zagury [Za66], Vik [Vi67], Adler [Ad68], and others. It is remarkable that a hadronic description of the excitation of the first excited state of the nucleon can succeed down to distance scales $q^2 \sim 100\,\text{fm}^{-2}$.

[7] In $d\sigma_{\text{el}}$ the factors $\sigma_{\text{Mott}} r$ are evaluated at the same (ε_1, θ) while $w_{1,2}(q^2)_{\text{el}}$ are evaluated at the resonance peak. The resulting ratio in Fig. 12.9 is essentially independent of θ for small θ and all the $q^2 \neq 0$ points [Wa72].

https://doi.org/10.1017/9781009290616.015 Published online by Cambridge University Press